International Immunopharmacology 70 (2019) 396–407

Contents lists available at ScienceDirect

International Immunopharmacology

journal homepage: www.elsevier.com/locate/intimp

Indirubin-3′-monoxime prevents aberrant activation of GSK-3β/NF-κB and alleviates high fat-high fructose induced Aβ-aggregation, gliosis and apoptosis in mice brain

C. Sathiya Priya, R. Vidhya, K. Kalpana, C.V. Anuradha*

Department of Biochemistry and Biotechnology, Annamalai University, Annamalai Nagar, Tamil Nadu, India

ARTICLE INFO

Keywords:
HFFD
Amyloid
Indirubin-3′-monoxime
Glycogen synthase kinase-3β
Nuclear factor kappa B
Neuroinflammation

ABSTRACT

Deciphering the molecular mechanisms of amyloid pathology and glial cell-mediated neuroinflammation, offers a novel avenue for therapeutic intervention against neurodegeneration. Recent findings demonstrate a crucial link between activation of glycogen synthase kinase-3β (GSK-3β), amyloid deposition and a neuroinflammatory state. However, studies demonstrating the pharmacological effects of GSK-3β inhibition and the interlinked molecular mechanisms still remain elusive. The present study explores whether high fat-high fructose diet (HFFD)-induced neuropathological changes could be alleviated by indirubin-3′-monoxime (IMX), a GSK-3β inhibitor. Male Swiss albino mice (8 weeks old) were fed with normal pellet or HFFD for 60 days. HFFD mice were treated with IMX once daily for last 7 days of the experimental period. HFFD fed-mice had significant amyloid deposits in cerebral cortex and hippocampus, and protein expression analyses showed activation of GSK-3β, nuclear translocation of NF-κB p65 and upregulation of inflammatory (TNF-α, IL-6, COX-2), astrocytic (GFAP), glial surface (CD-68) and pro-apoptotic markers (Bax and caspase-3). IMX treatment promotes the inhibitory phosphorylation of GSK-3β at Ser^{9} and moreover, a marked reduction in the phosphorylation of IKK-β, which prevents translocation and activation of NF-κB. Protein expression studies in IMX-treated brain tissues positively correlate with the anti-neuroinflammatory effects of GSK-3β inhibition. Taken together, our results provide substantial evidence that IMX could potentially attenuate neuroinflammation in coordination with the master transcription factor-NF-κB.

1. Introduction

Consumption of diet rich in saturated fats and refined sugars is associated with development of neurodegenerative diseases, characterized by accumulation of the toxic amyloid beta (Aβ) peptides, chronic inflammation, and neuronal loss [1–3]. Aβ peptides are generated from the amyloid precursor protein (APP) upon cleavage by the proteolytic activities of β- and γ-secretases [4]. APP has been implicated as a regulator of synapse formation, neural plasticity and memory [5,6]. However, overexpression and metabolic processing of APP by β- and γ-secretases generate toxic amyloid peptides ($Aβ_{1–40}$ and $Aβ_{1–42}$). Compelling evidence indicates that formation of senile plaques composed of Aβ-peptides can induce neuroimmune response by the immunocompetent glial cells, predominantly astrocytes and microglia. Chronic glial cell activation releases proinflammatory and neurotoxic factors such as tumor necrosis factor (TNF-α), interleukin (IL-6), nitric oxide (NO), cyclooxygenase-2 (COX-2) and reactive oxygen species (ROS) which result in neuronal dysfunction [7].

Glycogen synthase kinase-3β (GSK-3β) is an evolutionarily conserved serine/threonine kinase that plays multifaceted role in diverse cellular and neurophysiological processes [8]. GSK-3β is regulated by inhibitory serine and stimulatory tyrosine phosphorylation on Ser^{9} and Tyr^{216} respectively [9]. Dysregulation of GSK-3β has been implicated in diabetes [10], mood disorders [11] and Alzheimer's disease (AD) [12]. Active GSK-3β in brain stimulates the molecular machinery responsible for amyloid deposition and microglia-mediated neuroinflammation [13], and is pro-apoptotic [14]. Conversely, treatment with GSK 3β inhibitor has been reported to prevent Aβ accumulation in transgenic mice over-expressing GSK3β [12]. Inhibition of GSK-3β using short interference RNA (SiRNA) reduced NO production, but increased expression of IL-10 in both BV-2 cells and primary rat microglia cultures [15]. Since vast number of signaling pathways converge on GSK-3β, GSK-3β has turned out to be an important therapeutic target.

Indirubin extracted from the plants such as *Polygonum tinctorium*

* Corresponding author at: Department of Biochemistry and Biotechnology, Annamalai University, Annamalai Nagar 608 002, Tamil Nadu, India.
E-mail address: cvaradha975@gmail.com (C.V. Anuradha).

https://doi.org/10.1016/j.intimp.2019.02.053
Received 4 December 2018; Received in revised form 13 February 2019; Accepted 28 February 2019
Available online 08 March 2019

and *Isatis indigotica* or the gastropod molluscs of the Muricidae family (*Hexaplus trunculus and Morula granulata*) has been used as an active ingredient in traditional Chinese medicine to prevent inflammatory diseases and leukemia [16,17]. Indirubin derivatives have been shown to inhibit cyclin dependent kinase-5 and GSK3β activities [18]. Studies reveal that indirubin-3′-monoxime (IMX) can pass blood brain barrier (BBB) [19], can attenuate amyloid toxicity and neuronal apoptosis *in vitro* [20,21] and prevent memory deficits *in vivo* [22]. The underlying molecular mechanisms behind the neuroprotective effects of IMX in rodent models still remain largely unknown. The present study aims to explore the extent of neuropathological changes induced by a combination of high fat-high fructose diet, and to resolve the effects of IMX intervention on amyloid deposition and glial cell-mediated neuroinflammation and apoptosis.

2. Materials and methods

2.1. Chemicals, reagents and antibodies

Fructose was obtained from SFA Food and Pharma Ingredients Pvt. Ltd., Thane, Maharashtra and casein was bought from Clarion Casein Pvt. Ltd., Kadi, Gujarat. Indirubin-3′-monoxime was purchased from Cistron Biolab Pvt., Ltd., Chennai, India. Protease inhibitor cocktail (P8340), β-actin antibody (A2228) and FITC-conjugated-anti-rabbit secondary antibody (F0382), Amersham Hybond PVDF membranes (GE10600086), Hoechst stain (H6024) and toluidine blue (89640) were purchased form Sigma-Aldrich Pvt. Ltd., St. Louis, MO. HRP- conjugated anti-rabbit secondary antibody (#7074) and antibodies for GSk3β (#12456), p-GSK-3β Ser^9 (#5558), inhibitor of κappa B kinase-β (IKK-β) (#2678), p-IKK-β (#2697), nuclear factor kappa B (NF-κB) p65 (#8242) and Histone H3 (#4499) were purchased from Cell Signaling Technologies, Danvers, MA. Antibodies for TNF-α (sc-52746), IL-6 (sc-28343), COX-2 (sc-376861), Bcl-2-associated X (Bax) protein (sc-7480), B-cell lymphoma (Bcl)-2 (sc-7382) and caspase-3 (sc-271028) antibodies were purchased from Santa Cruz Biotechnology, Santa Cruz, *CA*. Antibodies for glial fibrillary acidic protein (GFAP) (BSB 5566) and cluster of differentiation (CD)-68 (BSB 5293) were purchased from Bio SB, Santa Barbara, CA, USA. Anti-mouse (HPO4) secondary antibody was purchased from Genei Laboratories Pvt. Ltd., Bengaluru, India. The pierce™ enhanced chemiluminescence (ECL) Western blotting substrate (32209) was purchased from Thermo Fisher Scientific, Rockford, USA. Congo red dye (573-58-0) was purchased from Loba Chemie Pvt. Ltd., Mumbai, India. Mayer's Hematoxylin (48441) was purchased from Sisco Research Laboratories Pvt. Ltd., Mumbai, India. Propidium iodide (PI) (ML067), bovine serum albumin (BSA) (MB083), solvents and other chemicals used for the study were purchased from Himedia Laboratories Pvt. Ltd., Mumbai, India.

2.2. Animals and ethics statement

Male Swiss albino mice (7 weeks old) were purchased from Biogen Laboratory Animal Facility, Bengaluru, India. Animals were acclimated for a week, weighed and maintained according to the Animal Care and Use Guidelines, Committee for the Purpose of Control and Supervision of Experiments on Animals (CPCSEA), in the Central Animal House, Unit of Experimental Medicine, Rajah Muthiah Medical College and Hospital, Annamalai University. The animals were housed in a temperature- and humidity-controlled environment and given access to feed and water *ad libitum*. Experimental protocols were approved by the Institutional Animal Ethical Committee (IEAC), Annamalai University [Reg.no.160/1999/CPSEA, Proposal No: 1133].

2.3. Grouping and treatment schedule

Mice (8 weeks old) were randomly grouped and treated as follows: Group I- Control, Group II- HFFD and Group III- HFFD + IMX. Three groups of six mice each ($n = 18$) were maintained for 60 days and fed with either normal pellet or HFFD. HFFD was prepared fresh in our laboratory every week with 45% fructose, 20% fat (10% beef tallow, 10% groundnut oil) and 22.5% casein, providing 471.25 cal/100 g. The pellet feed had 60% starch, 22.08% protein and 4.38% fat and provided 382.61 cal/100 g.

Table 1
Body weight of experimental animals.

Body Weight	Control	HFFD	HFFD + IMX
Initial (g)	24.1 ± 1.18	24.3 ± 1.27	24.5 ± 1.46
Final (g)	28.6 ± 1.20	34.9 ± 1.32[#]	31.3 ± 1.41[#,♣]

Values are means ± SD of six mice from each group.
[#] Significant *vs* Control.
[♣] Significant *vs* HFFD ($p < 0.05$).

IMX (0.4 mg/kg bw in 2.5% DMSO in saline, i.p.) was given once daily to HFFD-fed mice for last 7 days of the experimental period. The dosage of IMX was set from an earlier study [23]. At the end of the experimental period, mice (16.5 weeks old) were weighed, fasted overnight, anesthetized the next day *via* ketamine injection and euthanized. For western blotting experiments, the brain tissues ($n = 3$ from each group) were immediately excised under sterile condition into a dish with ice-cold PBS (pH -7.4) and washed three times with PBS. The dish was kept on ice cubes and the tissues after washing were stored at −80 °C. For histology studies, brain tissues ($n = 3$ from each group) were fixed in freshly prepared 10% neutral buffered formalin, and processed for paraffin embedding.

2.4. Immunoblotting

Brain homogenates were prepared using ice-cold homogenization buffer (50 mM Tris, 0.25% SDS, 150 mM NaCl, 1% NP-40 and 1 mM EDTA, pH 7.4) and centrifuged at 4 °C for 15 min at 10,000 × *g*. For analysis of NF-κB p65, nuclear fraction was extracted using kit from Cayman Chemical Company, MI, USA. Equivalent quantity of total protein (50 μg/lane) or nuclear protein (for NF-κB p65 and Histone H3), were separated on 12.5% (for NF-κB p65 and Histone H3), 12% (for Bax and Bcl-2,), 10% (for GSK-3β, p-GSK-3β and β-actin) or 8% (for IKK-β and p-IKK-β) polyacrylamide gel and then transferred onto polyvinylidene difluoride membranes. The membranes were incubated for 2 h in blocking solution [3% BSA in tris buffered saline containing Tween-20 (TBST)] and then washed thrice in TBST before overnight incubation at 4 °C with primary antibodies in appropriate dilution (1:1000 for GSK-3β, p-GSK-3$β^{ser9}$, IKK-β and p-IKK-β; 1:200 for NF-κB p65, Bax and Bcl-2). To remove excess primary antibody, membranes were washed with TBST on the next day and were incubated for 2 h with horseradish peroxidase (HRP)-conjugated anti-rabbit or anti-mouse secondary antibody (1:1000). Protein expression was detected using chemiluminescence substrate and the luminescence glow was captured in a gel documentation system (GELSTAN Chemi, Medicare Scientific supplies, India). The intensity of bands in each lane was detected using Image J software (National Institute of Health, Bethesda, USA). For normalization, the membranes were stripped and reprobed with antibodies for IKK-β, GSK-3β, Histone H3 or β-actin antibody.

2.5. Toluidine blue and congo red staining

The coronal sections of mice brain (4 μm thickness) were deparaffinized in xylene and treated with graded concentrations of alcohol followed by washing in distilled water. From this point onwards the slides were processed further for toluidine blue or congo red staining. The slides from each group were incubated with toluidine blue stain (stock: 1 mg/ml in 70% ethanol; working: 1 ml stock diluted with 9 ml of 1% NaCl. pH 2.3 ~ 2.5) for 10 min and washed in distilled water,

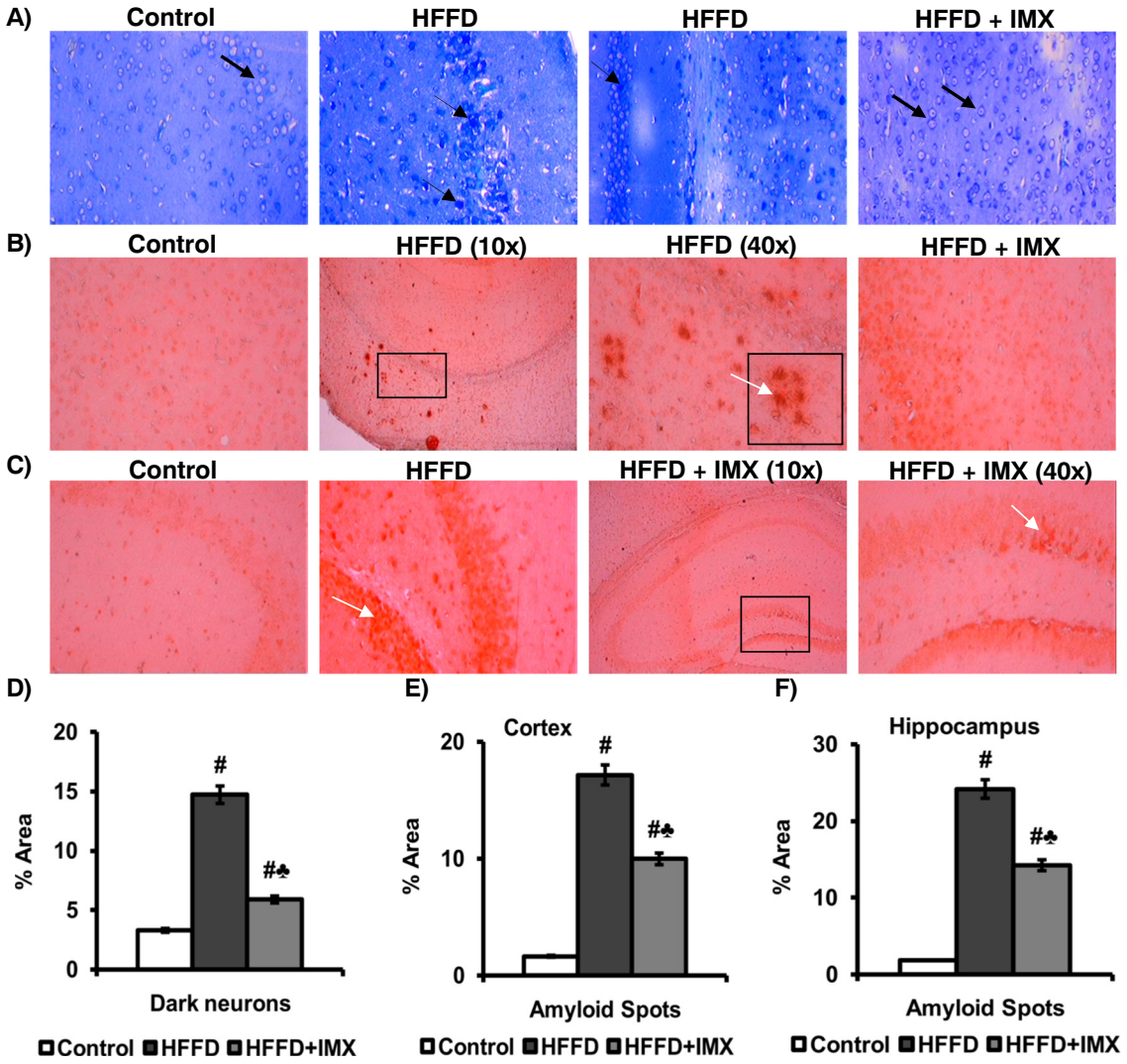

Fig. 1. (A) Toluidine blue stained sections of mice brain showing normal cells (thick arrows) and dark neurons (thin arrows). (B and C) Congo red stained sections of mice brain showing amyloid deposits (white arrows). (D) Area occupied by toluidine blue positive cells. (E and F) Area occupied by congo red positive amyloid spots in cortex and hippocampus. Mean ± SD of 4 view fields/coronal brain section [$n = 3$, tissue sections from three animals in each group]. One way ANOVA followed by Tukey test, $p < 0.05$. #Significant *vs* Control; ♣Significant *vs* HFFD. (For interpretation of the references to colour in this figure legend, the reader is referred to view web version of this article.)

dehydrated and mounted with coverslips. Four images (40×) from cortical and hippocampal region of coronal brain section ($n = 3$, tissue sections from three animals in each group) were analyzed using Image J software to obtain % area occupied by toluidine blue positive karyopyknotic dark neurons. For congo red staining, the sections from each group were incubated for 20 min at room temperature with congo red (0.5% in 50% ethanol, prepared fresh). The slides were then dipped for 2–3 times in alkaline alcohol solution (1%NaOH and 50% ethanol (1:100), prepared fresh) followed by washing in distilled water, dehydrated and mounted with cover slips. Four images (40×) from cortical and hippocampal region of coronal brain section ($n = 3$, tissue sections from three animals in each group) were analyzed using Image J software to obtain % area occupied by congo red positive amyloid spots. Images were captured in an Olympus microscope (CX41) with objective lens (10× or 40×) and eye piece (10×) to provide a total magnification of 100× or 400 × .

2.6. Immunohistochemistry

The paraffin sections were deparaffinized, treated with alcohol, washed and boiled for antigen retrieval in citrate buffer (pH -6.0) with Tween-20. The slides were then washed in TBS (pH -7.6) and treated with 0.3% hydrogen peroxide for 15 min to remove the endogenous peroxidase. Slides were incubated for blocking with 3% BSA for 2 h at room temperature followed by overnight incubation with primary antibody against p-IKK-β, TNF-α, IL-6, COX-2, GFAP, CD-68, Bax, Bcl-2 and caspase-3 (1:200). Binding of primary antibody was detected using HRP-conjugated anti-rabbit or anti-mouse secondary antibody. Immunopositive cells were visualized using the chromogenic substrate diaminobenzene (DAB). The slides were then counterstained with Mayer's Hematoxylin, washed, dried and mounted. All sections from each group were processed under same conditions in the same running with same antibody concentration, in order to make the immunostaining comparable between the groups. Images were captured using Olympus microscope (CX41) with a 40× objective and a 10× eye piece to provide total magnification of 400×. Four images (40×) from cortical and hippocampal region of coronal brain section ($n = 3$, tissue sections from three animals in each group) were examined using Image J software to obtain % area of immunoreactivity.

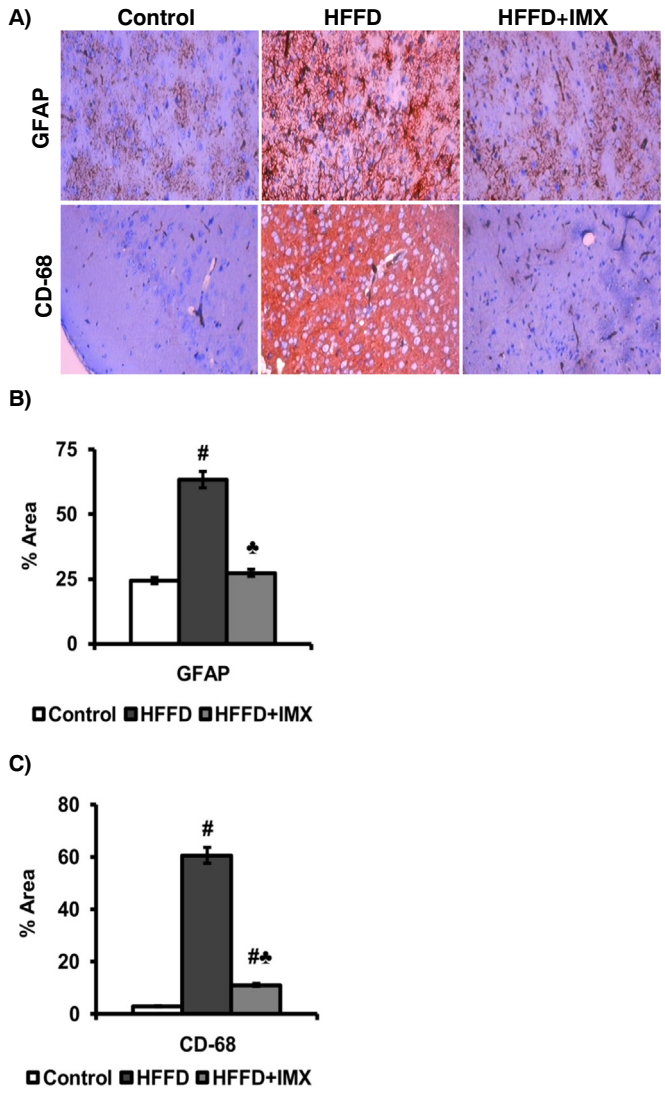

Fig. 2. (A) Immunohistochemical staining of astrocytes and microglia with GFAP and CD-68 antibodies (40×). Dense positive DAB staining indicates glial cell activation. (B and C) Area occupied by GFAP and CD-68 immunoreactivity. Mean ± SD of 4 view fields/coronal brain section [$n = 3$, tissue sections from three animals in each group]. One way ANOVA followed by Tukey test, $p < 0.05$. #Significant *vs* Control; ♣Significant *vs* HFFD. (For visualization of peroxidase-DAB reaction product, the reader is referred to view web version of this article).

2.7. Immunofluorescence

The tissue sections were deparaffinized, treated with alcohol and washed in distilled water. After antigen retrieval, the slides were blocked with 3% BSA for 1 h at room temperature. After blocking, the slides were incubated overnight at 4 °C with the primary antibodies, pGSK-3β or NF-κB p65 (1:200). Following three washes with TBS, the sections were incubated with anti-rabbit IgG-FITC secondary antibody (1:80) for 1 h at room temperature. After washing out the excess unbound secondary antibody, sections were incubated with nuclear counterstain (Hoechst or PI). Images were captured using EVOS FLoid cell imaging station with 20× fixed fluorite objective (Life Technologies, CA, USA). Four images (20×) from cortical and hippocampal region of coronal brain section ($n = 3$, tissue sections from three animals in each group) were examined using Image J software to obtain fluorescence intensity.

2.8. Statistical analysis

Results were analyzed using SPSS software, version 20 (SPSS Inc., Chicago, IL, USA) and comparisons were made by one-way ANOVA followed by Tukey *post hoc* test. The values represent means ± SD of three mice from each group for western blotting. For histological determinations, % area and fluorescence intensity are expressed as values representing mean ± SD of four images from cortical and hippocampal regions of coronal brain section ($n = 3$, tissue sections from three animals in each group). $P < 0.05$ were considered statistically significant.

3. Results

3.1. Body weight of experimental animals

The body weight of the animals was recorded at the start and at the end of the experimental period. After 60 days of experimental period, HFFD mice showed evidence of significant weight gain (by 18%) when compared to control mice. Upon IMX administration, HFFD-induced weight gain was considerably decreased (by 10%) as compared to IMX untreated HFFD-fed animals. Data are presented in Table 1.

3.2. IMX attenuates production of dark neurons in brain of HFFD mice

To examine the proportion of degenerating dark neurons, toluidine blue staining was carried out. The percentage area occupied by dark neurons was significantly increased in HFFD mice (by 11.4%) and the neurons were characterized by condensation of cellular components and shrinkage, when compared to the control mice. IMX injection to HFFD mice decreased the area occupied by dark neurons (by 8.8%), when compared to HFFD mice (Fig. 1A, D).

3.3. IMX clears HFFD-induced amyloid plaques

To identify amyloid deposition, brain tissue sections were stained with congo red dye. As seen in Fig. 1B, C, E, F mice fed HFFD for 60 days show significant increase in percentage area occupied by amyloid spots (by 15.5% in cortex and 22.3% in hippocampus) when compared to the control mice. Further, the reddish amyloid deposits are more prominent in cortex (cored type) than in hippocampus (granular type). In IMX-treated HFFD mice, the amyloid spots are remarkably decreased (by 7.1% in cortex and 9.9% in hippocampus when compared to HFFD mice) and mildly stained similar to that of control mice.

3.4. IMX reverses HFFD-induced glial cell activation

To assess the status of glial cell activation, protein expression of the astrocytic (GFAP) and glial surface (CD-68) markers were analyzed by immunohistochemistry. Brain tissues from HFFD mice depict intense staining, showing increase in area of immunoreactivity for reactive astrocytes and microglia (by 39% and 57.7% respectively) than control mice. Subsequent to clearance of amyloid plaques, immunopositive area for GFAP and CD-68 were significantly decreased in IMX treated mice (by 36% and 49.5% respectively when compared to HFFD mice) proving attenuation of gliosis (Fig. 2A–C).

3.5. IMX inhibits HFFD-induced GSK-3β activation

As GSK-3β is the key player involved in amyloid deposition as well as glial cell activation, we next sought to investigate the phosphorylation status of GSK-3β by immunoblotting and immunofluorescence analysis. The inhibitory phosphorylation of GSK-3β at Ser 9 was significantly decreased in brain tissues of HFFD-fed mice implying GSK-3β activation. Amyloidosis and gliosis might be prompted as a consequence of active GSK-3β in HFFD mice. Further, IMX administration to HFFD mice significantly improved the phosphorylation status of GSk-

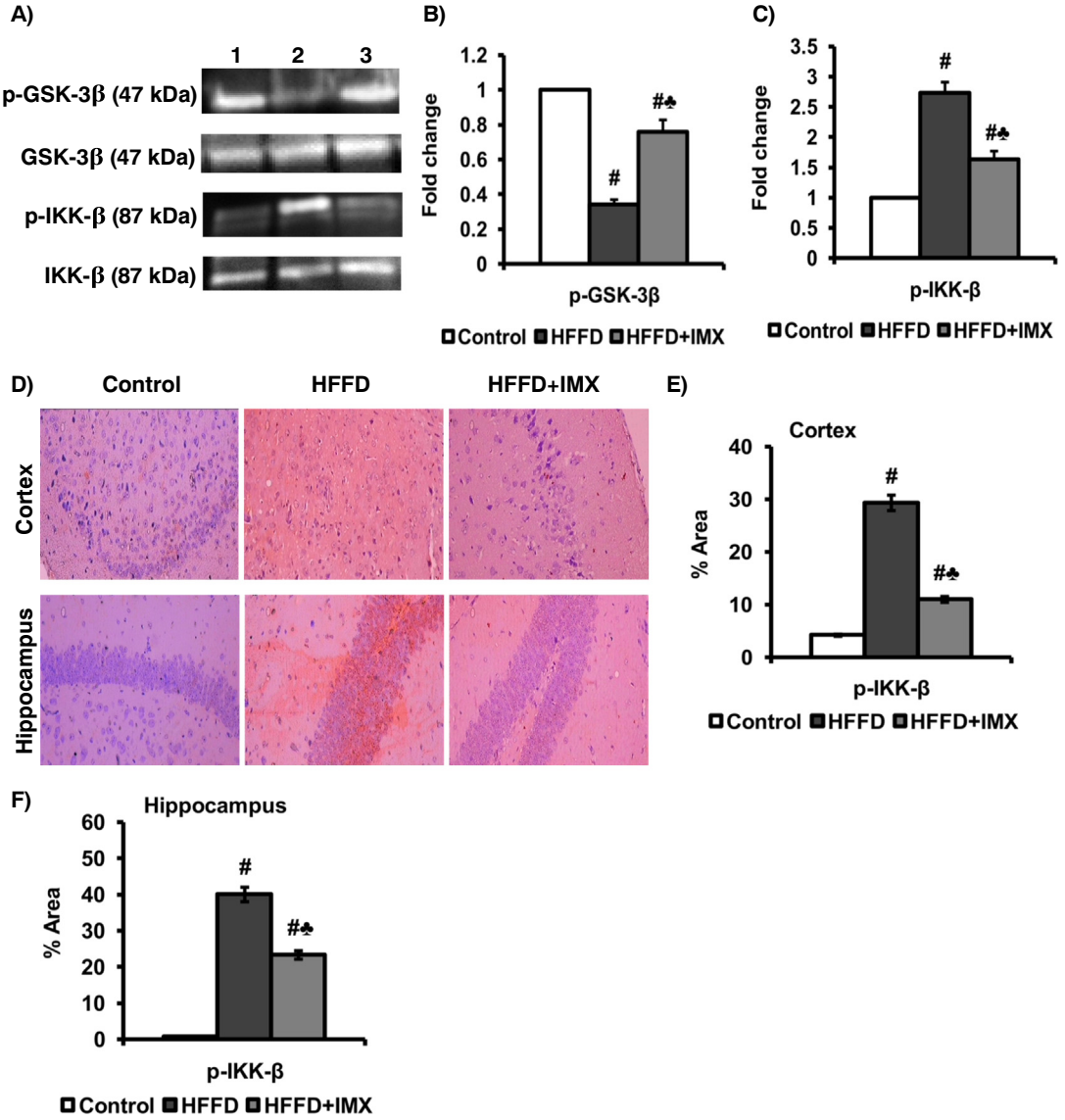

Fig. 3. (A) Immunoblots for p-GSK-3β and p-IKK-β in brain tissue. (B and C) Densitometry data expressed as fold change with respect to control. Values represent means ± SD (n = 3). (D) Immunohistochemical localization of p-IKK-β, (40×). (E and F) Area occupied by p-IKK-β immunoreactivity in cortex and hippocampus. Mean ± SD of 4 view fields/coronal brain section [n = 3, tissue sections from three animals in each group]. One way ANOVA followed by Tukey test, $p < 0.05$. #Significant *vs* Control; ♣Significant *vs* HFFD. (For visualization of peroxidase-DAB reaction product, the reader is referred to view web version of this article).

3β to attenuate HFFD-induced neuropathological changes (Fig. 3A and B). The mean intensity for pGSK3β/FITC in HFFD mice was found to be decreased (11.23 in cortex and 9.19 in hippocampus) when compared to control mice (30.98 in cortex and 24.29 in hippocampus), while IMX treated group showed increase in mean fluorescence intensity (19.27 in cortex and 16.7 in hippocampus) when compared to IMX untreated HFFD-fed animals (Fig. 4A–D).

3.6. IMX blunts IKK-β/NF-κB signaling in HFFD-fed mice

As GSK-3β activation is known to be associated with inflammatory conditions, we next examined the phosphorylation status of IKK-β and nuclear translocation of NF-κB p65. Protein expression analysis in HFFD mice brain reveals increase in the levels of p-IKK-β when compared to control and IMX treatment to HFFD mice significantly decreased the levels of p-IKK-β (Fig. 3A and C). The percentage area of p-IKK-β immunoreactivity in brain tissues of HFFD mice was increased (by 25.1% in cortex and 39.3% in hippocampus) as compared to control mice, whereas in the IMX treated group, the intensity of p-IKKβ staining was decreased (by 18.3% in cortex and 16.7% in hippocampus when compared to HFFD mice) (Fig. 3D–F). These results corroborate with those obtained in immunoblotting analysis of p-IKK-β.

Concordant with the phosphorylation status of IKK-β, NF-κB p65 expression in nuclear extracts were also increased in HFFD mice as compared to control mice. IMX treatment to HFFD mice significantly lowered the nuclear accumulation of NF-κB p65 when compared to HFFD mice (Fig. 5A, B). Further, immunofluorescence analysis of NF-κB p65/FITC in brain of HFFD mice confirms nuclear localization, and the mean intensity was found to be increased (28.0 in cortex and 33.1 in hippocampus) when compared to control (18.1 in cortex and 24.4 in hippocampus). Interestingly, the intensity of NF-κB p65/FITC staining in HFFD + IMX group was reduced (22.3 in cortex and 27.3 in hippocampus) when compared to IMX untreated HFFD-fed animals and was confined to cytoplasm (Fig. 5C–F).

3.7. IMX downregulates HFFD-induced pro-inflammatory mediators

After analysing NF-κB activation, we next aimed to examine the

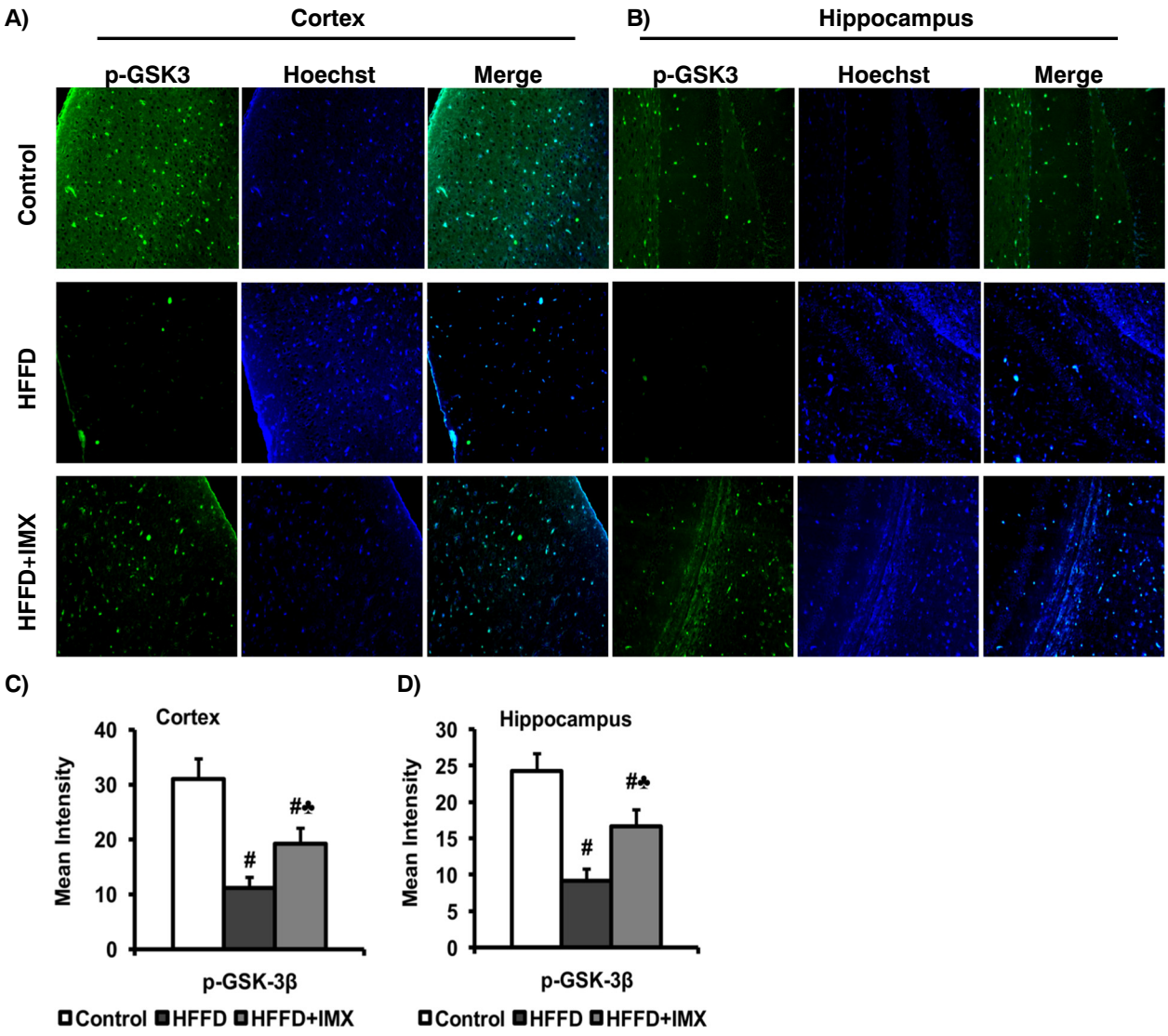

Fig. 4. (A and B) Immunofluorescence detection of p-GSK-3β/FITC (green) and Hoechst (blue) in cortex and hippocampus (20×). (C and D) Intensity of p-GSK-3β immunoreactivity in cortex and hippocampus. Mean ± SD of 4 view fields/coronal brain section [n = 3, tissue sections from three animals in each group]. One way ANOVA followed by Tukey test, $p < 0.05$. #Significant *vs* Control; ♣Significant *vs* HFFD. (For interpretation of the references to colour in this figure legend, the reader is referred to view web version of this article.)

protein expression of NF-κB-targeted pro-inflammatory mediators. Protein expression of TNF-α, IL-6 and COX-2 in mice brain are shown in Fig. 6A, B. Immunopositive area for TNF-α, IL-6 and COX-2 expression in HFFD group was increased in cortex (by 29.8%, 44.8% and 40.1% respectively) and in hippocampus (by 25%, 26.3% and 56.2% respectively) further supports the notion of NF-κB activation. IMX-administered HFFD group showed decrease in area of immunoreactivity for TNF-α and IL-6 in cortex (by 13.5% and 36.7% respectively) and in hippocampus (by 19% and 18.2% respectively) suggests its anti-neuroinflammatory functions. However, upregulation of COX-2 induced by HFFD was not significantly attenuated by IMX treatment. Upon IMX treatment 1.6% and 3.6% decrease was observed for area of COX-2 immunoreactivity in cortex and hippocampus respectively (Fig. 6C-H).

3.8. IMX prevents HFFD-induced neuroapoptosis

Following assessment of neuroinflammatory molecules, the pro- (Bax and caspase-3) and anti-apoptotic proteins (Bcl-2) were observed in brain of experimental animals. The protein expression of Bax was increased in HFFD mice whereas Bcl-2 protein was found to be decreased. IMX treatment significantly decreased the levels of Bax, and upregulated Bcl-2, substantiate its anti-apoptotic effects (Fig. 7A–C). The immunohistochemical staining of Bax and caspase-3 in HFFD brain was increased in cortex (by 25% and 37.3% respectively) and in hippocampus (by 15.08% and 28.7% respectively), whereas immunohistochemical staining of Bcl-2 was markedly decreased (by 16.9% in cortex and 13.9% in hippocampus). In IMX treated brain tissues, immunopositivity for Bax and caspase-3 was reduced in cortex (by 18.2% and 32.7% respectively) and in hippocampus (by 8% and 26.5% respectively), while immunopositivity for Bcl-2 was increased by 9% in cortex and 7.8% in hippocampus when compared to HFFD mice (Fig. 7D, E and Fig. 8A–F).

4. Discussion

The present study explored a cause-effect relationship between HFFD feeding and the extent of neuropathological changes in mice brain. Further, the ameliorative effects of the GSK-3β inhibitor IMX on amyloid deposition, glial cell-mediated neuroinflammation and apoptosis are investigated. The present study reports for the first time that

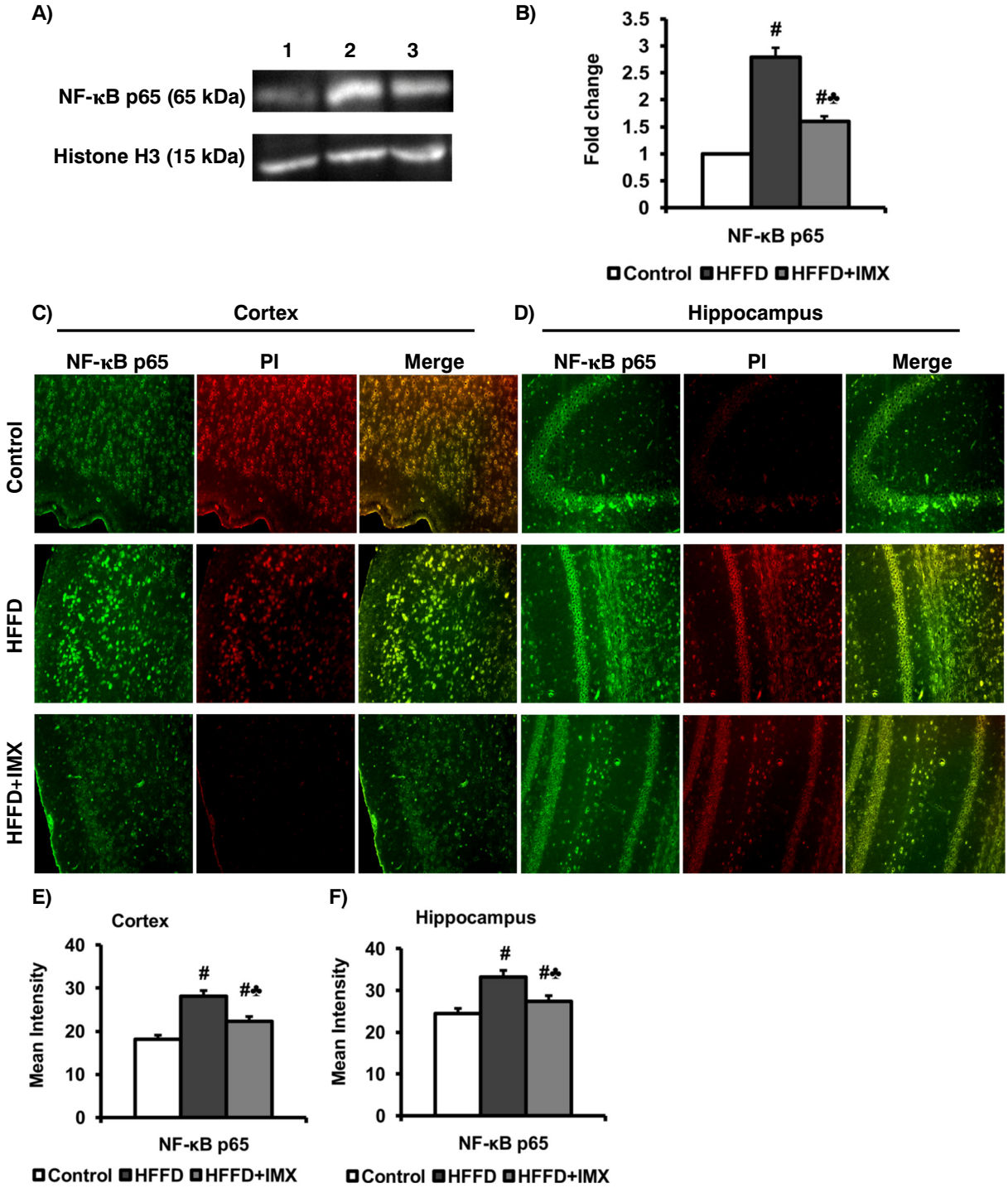

Fig. 5. (A) Immunoblots for NF-κB p65 in brain tissue. (B) Densitometry data expressed as fold change with respect to control. Values represent means ± SD (n = 3). (C and D) Immunofluorescence detection of NF-κB p65/FITC (Green) and PI (red) in cortex and hippocampus (20×). (E and F) Intensity of NF-κB immunoreactivity in cortex and hippocampus. Mean ± SD of 4 view fields/coronal brain section [n = 3, tissue sections from three animals in each group]. One way ANOVA followed by Tukey test, $p < 0.05$. #Significant *vs* Control; ♣Significant *vs* HFFD. (For interpretation of the references to colour in this figure legend, the reader is referred to view web version of this article.)

combination of high fat (20%) and high fructose (45%) diet when fed for 60 days can promote significant amyloid deposition in mice brain.

Previous studies from our laboratory have clearly documented that HFFD causes body weight gain and brings out metabolic changes (elevated levels of glucose, insulin, triglycerides, free fatty acids, total cholesterol, TNF-α and IL-6) in circulation and peripheral tissues [24–28]. Hematoxyin and eosin stained liver and kidney sections of HFFD mice displayed inflammatory infiltration of liver and kidney tubules and capsules (data not shown).

Neuronal function is compromised during calorie excess and in the long-term may potentiate neurodegeneration. Of late, HFD has been employed to study the pathogenesis of neurodegenerative diseases in metabolically challenged rodents [3,29] and few studies have also demonstrated the detrimental effects of sucrose/fructose to brain [30–32]. Diet rich in fat or simple sugars stimulate amyloid deposition and glial cell activation in brain [1,33–35], which are the hallmarks of AD [36].

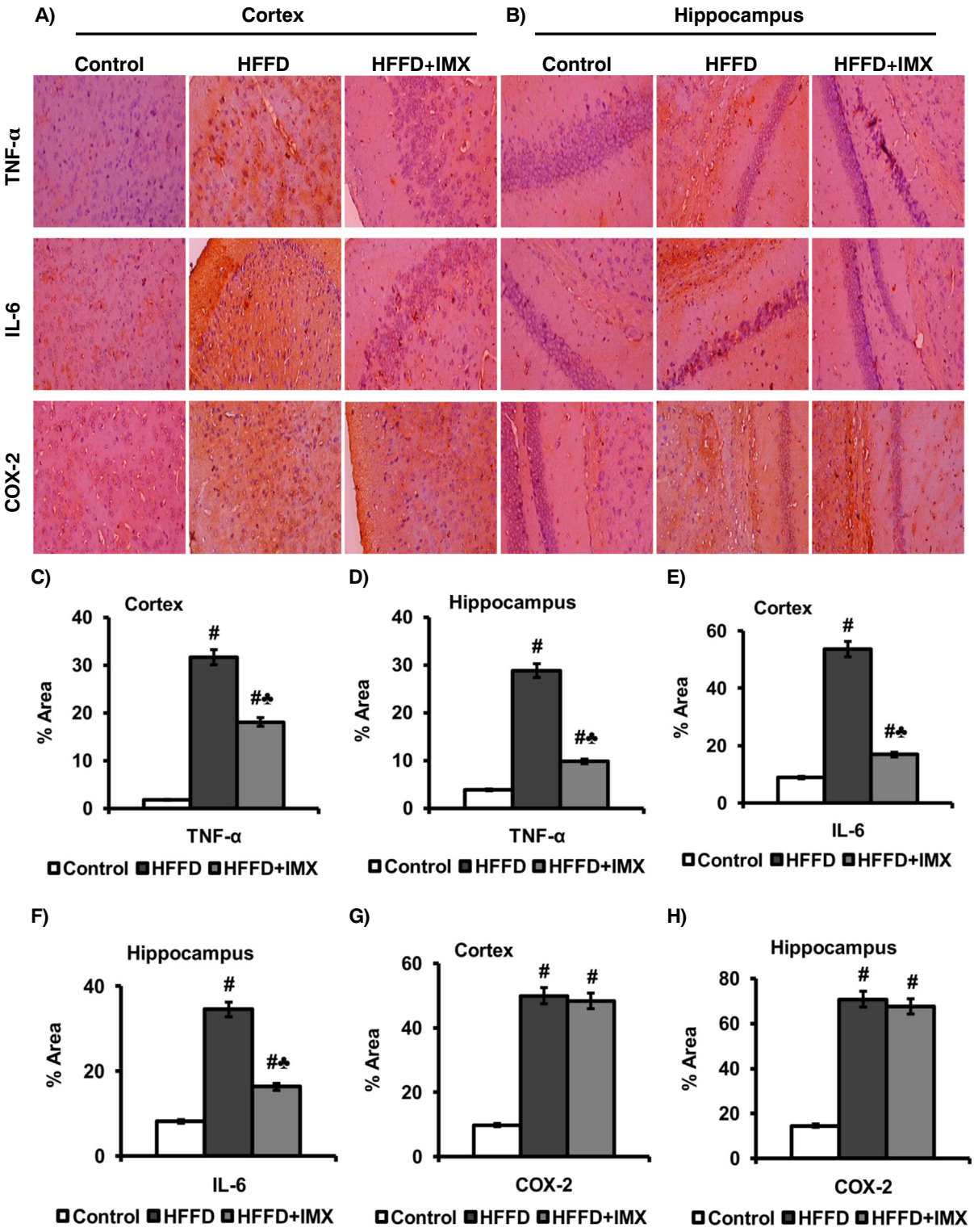

Fig. 6. (A and B) Immunohistochemical localization of TNF-α, IL-6 and COX-2 in cortex and hippocampus (40×). (C—H) Area occupied by TNF-α, IL-6 and COX-2 immunoreactivity. Mean ± SD of 4 view fields/coronal brain section [n = 3, tissue sections from three animals in each group]. One way ANOVA followed by Tukey test, $p < 0.05$. #Significant *vs* Control; ♣Significant *vs* HFFD. (For visualization of peroxidase-DAB reaction product, the reader is referred to view web version of this article).

Gut dysbiosis is one mechanism through which HFFD may promote neuroinflammation. Perturbations in gut microbial diversity (changes in Firmicutes *vs* Baceteriodetes ratio) can alter gut epithelial integrity [37,38], that can release proinflammatory cytokines and microbial endotoxins into systemic circulation [39]. Endotoxaemia and inflammation cause leaky blood brain barrier, accentuating neuroinflammatory response *via* toll-like receptors that contributes to Aβ deposition and glial cell activation [40].

Aβ accumulation provokes glial cell activation in mice hippocampus [41], and exert proinflammatory functions [42,43]. Aβ triggers transformation of quiescent glial cells to a reactive phenotype which clear Aβ aggregates and dead or dying neurons, but sustained activation

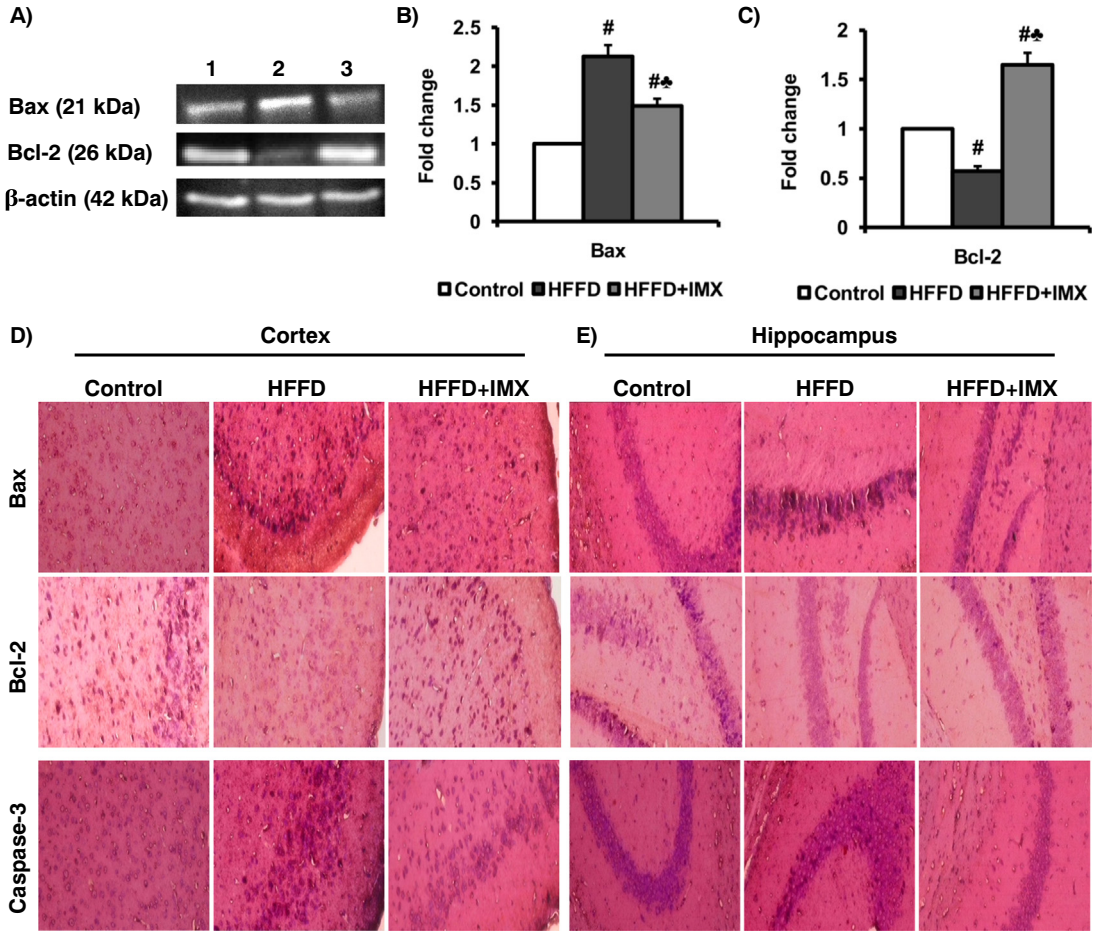

Fig. 7. (A) Immunoblots for Bax and Bcl-2 in brain tissue. (B and C) Densitometry data expressed as fold change with respect to control. Values represent means ± SD (n = 3). (D and E) Immunohistochemical localization of Bax, Bcl-2 and caspase-3 in cortex and hippocampus (40×). Mean ± SD of 4 view fields/coronal brain section [n = 3, tissue sections from three animals in each group]. One way ANOVA followed by Tukey test, $p < 0.05$. #Significant *vs* Control; ♣Significant *vs* HFFD. (For visualization of peroxidase-DAB reaction product, the reader is referred to view web version of this article).

result in loss of its phagocytic function, elevated secretion of neurotoxic substances and stimulation of Aβ synthesis [44]. Thus, Aβ deposition rewound neuronal injury, which in turn generates more Aβ resulting in a vicious cycle. Concomitant to amyloid deposition, intense DAB staining for immunohistochemical localization of GFAP and CD-68 in brain of HFFD mice was observed flaunting glial cell activation and proliferation.

Decreasing GSK-3β activity has therapeutic benefits in animal model of colitis [45] and traumatic brain injury [46] and ischemia/reperfusion injury [47,48]. In brain, activation of GSK-3β promotes Aβ toxicity by elevating APP expression and its amyloidogenic cleavage, and by dysregulating Aβ clearance mechanisms [49]. In HFFD fed mice, GSK-3β is active which might have triggered amyloid deposition. As a potential therapy for injurious stimuli induced by HFFD the beneficial effects of the GSK-3β inhibitor IMX has been investigated.

IMX has been shown to inhibit GSK-3β on binding to the catalytic site, by competing with ATP [50]. IMX inhibits Aβ-induced neurotoxicity in neuroblastoma cell lines [51] and stimulate the expression of the Aβ degrading enzymes, IDE and neprilysin in APP/PS1 mice [22]. IMX has been proposed to be a neuroprotective agent however the efficacy of IMX on Aβ-driven gliopathology and neuroinflammation induced by HFFD has not been studied so far. An intriguing finding of the present study is the effect of IMX on amyloid clearance. Our results reveal that IMX treatment could potentiate clearance of Aβ plaques induced by HFFD and this effect has been well correlated with potent inhibitory effect on GSK-3β. Nevertheless, the influence of IMX towards Aβ metabolism warrant future studies in this HFFD-model.

Previous studies demonstrate that IMX suppresses LPS-stimulated microglial cells [52] and attenuate astocytic/microglial activation in mouse model of AD [22]. In our study, IMX administration significantly decreased the protein expression of the astrocyte intermediate filament protein GFAP and the microglial surface maker CD-68. The results signify that IMX could suppress gliosis, and we speculate IMX may possibly reword amyloid clearance mechanisms.

Researchers emphasize critical roles for GSK-3β in facilitating NF-κB activation, as well as the induction of NF-κB targeted pro-inflammatory molecules [46,53]. GSK-3β activates NF-κB in LPS-stimulated RAW264.7 mouse macrophage cells [54] and positively regulates expression of pro-inflammatory genes in LPS-stimulated human monocytic cells and mouse hippocampal slice culture [52,55].

In order to ascertain the modulation of IKK-β/NF-κB signaling by HFFD and IMX, we assessed the phosphorylation status of the serine/threonine kinase IKK-β and protein expression of NF-κB p65 in nuclear extracts. IKK-β/NF-κB is a pluripotent master switch play role in classical immune response [56]. The prototypical NF-κB heterodimer consists of p50 and p65 subunits, which are sequestered in the cytoplasm through its association with IκB-α. Phosphorylation and activation of the stress kinase IKK-β phosphorylates its substrate IκB-α, which undergoes rapid ubiquitination and degradation. The dissociation of IκB-α allows NF-κB p60 and p65 to enter nucleus, where it binds to specific promoters to transcribe its downstream effectors like TNF-α, IL-6 and COX-2 [57].

In our study, HFFD feeding elicited activation of IKK-β by phosphorylation and orchestrated nuclear translocation of NF-κB p65 in

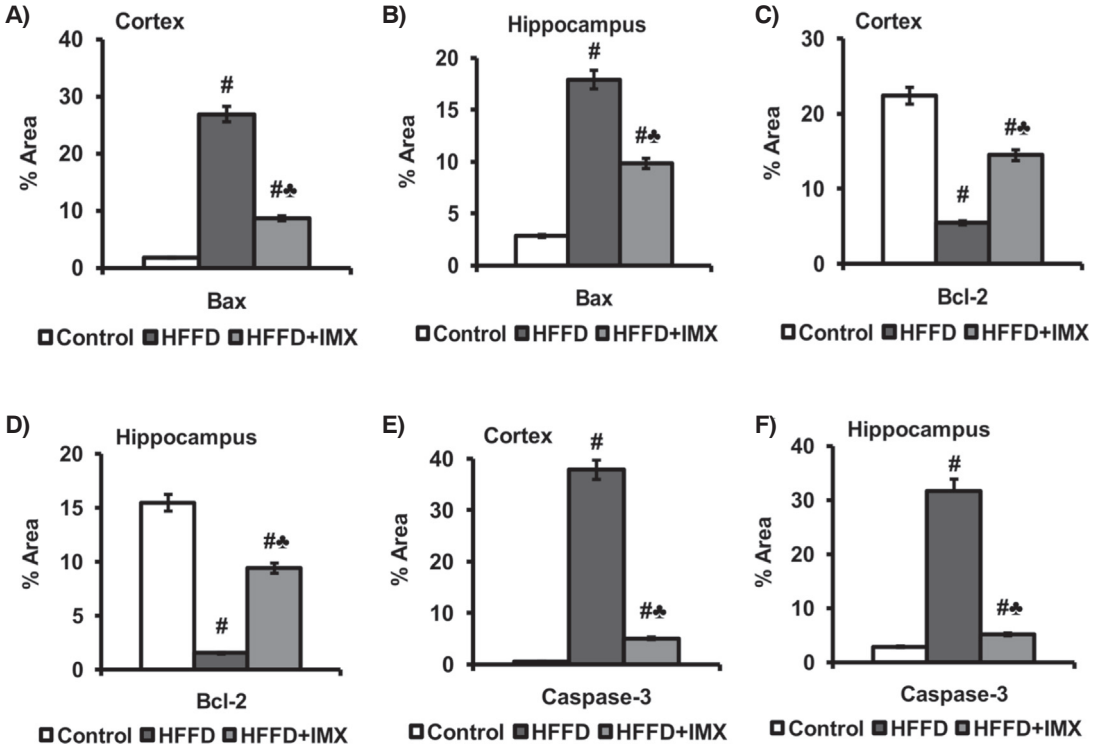

Fig. 8. (A-F) Area occupied by Bax, Bcl and caspase-3 immunoreactivity in cortex and hippocampus. Mean ± SD of 4 view fields/coronal brain section [n = 3, tissue sections from three animals in each group]. One way ANOVA followed by Tukey test, $p < 0.05$. #Significant *vs* Control; ♣Significant *vs* HFFD. (For visualization of peroxidase-DAB reaction product, the reader is referred to view web version of this article).

brain. Our results are consistent with a previous study which found that overnutrition can cause atypical activation of hypothalamic IKK-β/NF-κB [58]. The rise in immunopositive cells for TNF-α and IL-6 found in HFFD mice can be related to NF-κB activation as a sequel of amyloid deposition as reported previously [59–61]. Our results support previous observation documented that accumulation of Aβ-peptides promotes nuclear translocation of NF-κB and contributes to the generation of pro-inflammatory molecules [62].

IMX has been shown to inhibit NF-κB activation and JNK signaling to suppress the production of inflammatory mediators in LPS-treated RAW264.7 cells [63]. Similarly, treating HFFD mice with IMX reduced the levels of NF-κB p65 in nuclear extracts, and immunofluorescence images clearly depict cytoplasmic localization. Moreover, IMX treatment significantly decreased the protein expression of TNF-α and IL-6, which authenticates blockade of NF-κB signaling. IMX may suppress aberrant NF-κB signaling *via* IKK-β inactivation as revealed in the present study. The antiinflammatory effects of IMX and alleviation of metabolic perturbations in peripheral tissues of mice has been demonstrated [64,23]. IMX treatment was found to exert anti-inflammatory effect at peripheral tissues, liver and kidney as well (data not shown).

The expression of COX-2 has been correlated with the density of amyloid plaque [65]. A study reported that IMX was effective in suppressing the expression of iNOS and IL-6, but not COX-2, in LPS-stimulated BV2 microglial cells [52]. In this study, IMX did not alter upregulation of COX-2 induced by HFFD. We infer that IMX could attenuate neuroinflammation by blunting GSK-3β/NF-κB signaling without influencing COX-2.

Histopathological examination helps in evaluating neuronal damage and drug action. Dark neurons undergoing cytoskeletal and microfilament damage are diagnosed by its hyperbasophilic, hyperargyrophilic and high electron dense properties in histological sections under conditions of oxidative damage [66], diabetes [67], head injuries, ischemia and epilepsy [68]. In this study, we have identified more dark neurons in HFFD mice characterized by nuclear/cytoplasmic condensation with neuronal shrinkage. Further, IMX treatment significantly decreased the formation of dark neurons which clearly indicates its recuperative effects towards neuroapoptosis.

In our study, protein expression studies show upregulation of pro-apoptotic Bax protein with concomitant decrease in anti-apoptotic Bcl-2, signifying apoptosis activation in HFFD-fed mice. Our results corroborate with previous reports stating Aβ exposure induce mitochondrial dysfunction [69] and neuronal cell death [70]. Furthermore, in association with activation of GSK-3β in HFFD mice, the increase in Bax expression is correlated with a previous study demonstrating the role of GSK-3β in phosphorylation of Bax to promote neuronal apoptosis [71].

Activation of caspase-3 by Aβ-peptides induces apoptosis and contributes to the pathophysiology of AD [72,73]. Consistent with amyloid deposition, we have also found more number of caspase-3 positive cells in brain of HFFD mice, indicating accomplishment of neuroapoptosis. Previous studies indicate that GSK-3β inhibition by IMX protects neurons from apoptosis [20,51]. In our study, the anti-apoptotic effects of IMX are evident from the attenuation of Bax and caspase-3 expression along with an increase in Bcl-2. These results confirm the role of IMX in preventing intrinsic apoptosis and obviously the suppression of GSK-3β/NF-κB signaling seems to be the upstream event involved.

Taken together, we demonstrate that HFFD can induce Aβ-aggregation and neuroinflammation in mice brain. The exact mechanism for these neurodegenerative changes could be attributed by the activation of GS3β/NF-κB signaling. Our results provide robust evidence that HFFD intake for a long time can be a potential risk factor that increases the possibility of neurogenerative diseases such as AD. Hence dietary habits with low calorie foods are recommended. IMX treatment exerts potent neuroprotective effects *via* inactivation of NF-κB which is synchronized through the inhibition of GSK-3β. Derangements in brain insulin signaling dysregulate metabolic pathways of APP processing [74–76] and hence future studies uncovering the role of IMX on amyloid metabolism are of interest. Pharmacokinetic and toxicity studies

with IMX are sparse and hence recommended before initiating clinical trials.

Conflicts of interest

None.

Acknowledgement

We gratefully acknowledge the University Grants Commission, New Delhi, India for providing financial assistance to the first author Sathiya Priya C (Senior Research fellow, The Research Fellowship in Sciences for Meritorious Students, UGC-BSR scheme). The authors wish to thank DST-FIST and UGC-SAP for the facilities provided in Department of Biochemistry and Biotechnology, Annamalai University, Tamil Nadu, India.

References

[1] D. Cao, H. Lu, T.L. Lewis, L. Li, Intake of sucrose-sweetened water induces insulin resistance and exacerbates memory deficits and amyloidosis in a transgenic mouse model of Alzheimer disease, J. Biol. Chem. 282 (50) (2007) 36275–36282.
[2] L. Thirumangalakudi, A. Prakasam, R. Zhang, H. Bimonte-Nelson, K. Sambamurti, et al., High cholesterol-induced neuroinflammation and amyloid precursor protein processing correlate with loss of working memory in mice. J. Neurochem. 106 (2008) 475–485.
[3] D. Petrov, I. Pedrós, G. Artiach, F.X. Sureda, E. Barroso, M. Pallàsa, et al., High-fat diet-induced deregulation of hippocampal insulin signaling and mitochondrial homeostasis deficiences contribute to Alzheimer disease pathology in rodents, Biochim. Biophys. Acta, 1852 (2015) 1687–1699.
[4] V.W. Chow, M.P. Mattson, P.C. Wong, M. Gleichmann, An overview of APP processing enzymes and products, NeuroMolecular Med. 12 (2010) 1–12.
[5] P.R. Turner, K. O'Connor, W.P. Tate, W.C. Abraham, Roles of amyloid precursor protein and its fragments in regulating neural activity, plasticity and memory, Prog. Neurobiol. 70 (1) (2003) 1–32.
[6] C. Priller, T. Bauer, G. Mitteregger, B. Krebs, H.A. Kretzschmar, J. Herms, Synapse formation and function is modulated by the amyloid precursor protein, J. Neurosci. 26 (27) (2006) 7212–7221.
[7] W. Liu, Y. Tang, J. Feng, Cross talk between activation of microglia and astrocytes in pathological conditions in the central nervous system, Life Sci. 89 (2011) 141–146.
[8] R.S. Jope, C.J. Yuskaitis, E. Beurel, Glycogen synthase Kinase-3 (GSK3): inflammation, diseases, and therapeutics, Neurochem. Res. 32 (2007) 577–595.
[9] L. Kockeritz, B. Doble, S. Patel, J.R. Woodgett, Glycogen synthase kinase-3-an overview of an over-achieving protein kinase, Curr. Drug Targets 7 (2006) 1377–1388.
[10] H. Eldar-Finkelman, S.A. Schreyer, M.M. Shinohara, R.C. LeBoeuf, E.G. Krebs, Increased glycogen synthase kinase-3 activity in diabetes- and obesity-prone C57BL/6J mice, Diabetes 48 (1999) 1662–1666.
[11] X. Li, R.S. Jope, Is glycogen synthase kinase-3 a central modulator in mood regulation? Neuropsychopharmacology 35 (2010) 2143–2154.
[12] T. Engel, F. Hernandez, J. Avila, J.J. Lucas, Full reversal of Alzheimer's disease-like phenotype in a mouse model with conditional overexpression of glycogen synthase kinase-3, J. Neurosci. 26 (19) (2006) 5083–5090.
[13] C.A. Grimes, R.S. Jope, The multifaceted roles of glycogen synthase kinase 3 beta in cellular signalling, Prog. Neurobiol. 65 (4) (2001) 391–426.
[14] E. Beurel, R.S. Jope, The paradoxical pro- and antiapoptotic actions of GSK3 in the intrinsic and extrinsic apoptosis signaling pathways, Prog. Neurobiol. 79 (4) (2006) 173–189.
[15] W.C. Huang, Y.S. Lin, C.Y. Wang, C.C. Tsai, H.C. Tseng, C.L. Chen, et al., Glycogen synthase kinase-3 negatively regulates anti-inflammatory interleukin-10 for lipopolysaccharide-induced iNOS/NO biosynthesis and RANTES production in microglial cells, Immunology, 128 (1) (2009) e275–286.
[16] Z. Hu, Y. Tu, Y. Xia, P. Cheng, W. Sun, Y. Shi, L. Guo, H. He, C. Xiong et al., Rapid identification and verification of indirubin-containing medicinal plants, Evid. Based Complement. Alternat. Med., (2015) 484670.
[17] K. Benkendorff, D. Rudd, B.D. Nongmaithem, L. Liu, F. Young, et al., Are the traditional medical uses of Muricidae Molluscs substantiated by their pharmacological properties and bioactive compounds? Mar. Drugs, 13 (8) (2015) 5237–5275.
[18] L. Meijer, A.L. Skaltsounis, P. Magiatis, P. Polychronopoulos, M. Knockaert, M. Leost, et al., GSK-3-selective inhibitors derived from Tyrian purple indirubins, Cell Chem. Biol., 10 (2003) 1255–1266.
[19] M.L. Selenica, H.S. Jensen, A.K. Larsen, M.L. Pedersen, L. Helboe, et al., Efficacy of small-molecule glycogen synthase kinase-3 inhibitors in the postnatal rat model of tau hyperphosphorylation, Br. J. Pharmacol., 152 (2007) 959–979.
[20] Y. Xie, Y. Liu, C. Ma, Z. Yuan, W. Wang, et al., Indirubin-3′-oxime inhibits c-Jun NH2-terminal kinase: anti-apoptotic effect in cerebellar granule neurons, Neurosci. Lett., 367 (2004) 355–359.
[21] S. Zhang, Y. Zhang, L. Xu, X. Lin, J. Lu, et al., Indirubin-3-monoxime inhibits-amyloid-induced neurotoxicity in neuroblastoma SH-SY5Y cells, Neurosci. Lett. 450 (2009) 142–146.
[22] Y. Ding, A. Qiao, G. Fan, Indirubin-3′-monoxime rescues spatial memory deficits and attenuates β-amyloid-associated neuropathology in a mouse model of Alzheimer's disease, Neurobiol. Dis. 39 (2010) 156–168.
[23] S. Sharma, R. Taliyan, Neuroprotective role of Indirubin-30-monoxime, a GSKβ inhibitor in high fat diet induced cognitive impairment in mice, Biochem. Biophys. Res. Commun. 452 (2014) 1009–1015.
[24] S. Bhuvaneswari, E. Arunkumar, P. Viswanathan, C.V. Anuradha, Astaxanthin restricts weight gain, promotes insulin sensitivity and curtails fatty liver disease in mice fed a obesity-promoting diet, Process Biochem. 45 (2010) 1406–1414.
[25] E. Arunkumar, S. Bhuvaneswari, C.V. Anuradha, An intervention study in obese mice with astaxanthin, a marine carotenoid-effects on insulin signaling and pro-inflammatory cytokines, Food Funct. 3 (2012) 120–126.
[26] R. Geetha, B. Yogalakshmi, S. Sreeja, K. Bhavani, C.V. Anuradha, Troxerutin suppresses lipid abnormalities in the heart of high-fat-high-fructose diet-fed mice, Mol. Cell. Biochem. 387 (2014) 123–134.
[27] R. Geetha, M.K. Radhika, E. Priyadarshini, K. Bhavani, C.V. Anuradha, Troxerutin reverses fibrotic changes in the myocardium of high-fat high-fructose diet-fed mice, Mol. Cell. Biochem. 407 (2015) 263–279.
[28] R. Geetha, C. Sathiya Priya, C.V. Anuradha, Troxerutin attenuates diet- induced oxidative stress, impairment of mitochondrial biogenesis and respiratory chain complexes in mice heart, Clin. Exp. Physiol. Pharmacol. 44 (2017) 103–113.
[29] D. Wang, J.Y.J. Chen, W. Wu, X. Zhu, Y. Wang, Naringin improves neuronal insulin signaling, brain mitochondrial function, and cognitive function in high-fat diet-induced obese mice, Cell. Mol. Neurobiol. 35 (7) (2015) 1061–1071.
[30] K.V. derBorght, R. Köhnke, N. Göransson, T. Deierborg, P. Brundin, et al., Reduced neurogenesis in the rat hippocampus following high fructose consumption, Regul. Pept., 167 (1) (2011) 26–30.
[31] Z. Cai, Y. Zhao, S. Yao, B. Zhao, Increases in β-amyloid protein in the hippocampus caused by diabetic metabolic disorder are blocked by minocycline through inhibition of NFκB pathway activation, Pharmacol. Rep. 63 (2011) 381–391.
[32] C. Carvalho, S. Cardoso, C. Sónia, Correia, R. X, et al., Metabolic alterations induced by sucrose intake and Alzheimer's disease promote similar brain mitochondrial abnormalities, Diabetes, 61 (2012) 1234–1242.
[33] D. Luo, X. Hou, L. Hou, M. Wang, S. Xu, et al., Effect of pioglitazone on altered expression of Aβ metabolism-associated molecules in the brain of fructose-drinking rats, a rodent model of insulin resistance, Eur. J. Pharmacol. 664 (2011a) 14–19.
[34] P. Rivera, M. Perez-Martin, J. Francisco, Pavon, A. Serrano, et al., Pharmacological Administration of the Isoflavone Daidzein Enhances Cell Proliferation and Reduces High fat Diet-Induced Apoptosis and gliosis in the rat Hippocampus, PLoS One 8 (5) (2013) e64750.
[35] O. Busquets, M. Ettcheto, M. Pallàs, C. Beas-Zarate, E. Verdaguer, et al., Long-term exposition to a high fat diet favors the appearance of-amyloid depositions in the brain of C57BL/6J mice, a potential model of sporadic Alzheimer's disease, Mech. Ageing Dev., 162 (2017) 38–45.
[36] D. Kempuraj, R. Thangavel, G. P. Selvakumar, S. Zaheer, M.E. Ahmed, et al., Brain and peripheral atypical inflammatory mediators potentiate Neuroinflammation and neurodegeneration, Front. Cell. Neurosci., 11 (216) (2017).
[37] N.A. Ismail, S.H. Ragab, A.A. ElBaky, A.R.S. Shoeib, Y. Alhosary, D. Fekry, Frequency of Firmicutes and Bacteriodetes in gut microbiota in obese and normal weight Egyptian children and adults, Arch. Med. Sci. 7 (2011) 501–507.
[38] M.H. Do, E. Lee, M.J. Oh, Y. Kim, H.Y. Park, High glucose or –fructose diet cause changes of the gut microbiota and metabolic disorders in mice without body weight change, Nutrients 10 (2018) 1–14.
[39] C. Jiang, G. Li, P. Huang, Z. Liu, B. Zhao, The gut microbiota and Alzheimer's disease, J. Alzheimers Dis. 58 (2017) 1–15.
[40] V.V. Giau, S.Y. Wu, A. Jamerlan, S.S.A. An, S.Y. Kim, J. Hulme, Gut microbiota and their neuroinflammatory implications in Alzheimer's disease, Nutrients 10 (2018) 1–18.
[41] G.F. Passos, C.P. Figueiredo, R.D. Prediger, et al., Involvement of phosphoinositide 3-kinase gamma in the neuro-inflammatory response and cognitive impairments induced by beta-amyloid 1–40 peptide in mice, Brain Behav. Immun., 24 (2010) 493–501.
[42] F.Q. He, B.Y. Qiu, T.K. Li, Q. Xie, D.J. Cui, Tetrandrine suppresses amyloid-β- induced inflammatory cytokines by inhibiting NF-κB pathway in murine BV2 microglial cells, Int. Immunopharmacol. 11 (9) (2011) 1220–1225.
[43] W. Lin, M. Ding, J. Xue, W. Leng, The role of TLR2/JNK/NF-κB pathway in amyloid β peptide-induced inflammatory response in mouse NG108-15 neural cells, Int. Immunopharmacol. 17 (3) (2013) 880–884.
[44] F. Zhang, L. Jiang, Neuroinflammation in Alzheimer's disease, Neuropsychiatr. Dis. Treat. 11 (2015) 243–256.
[45] B.J. Whittle, C. Varga, A. Posa, A. Molnar, M. Collin, et al., Reduction of experimental colitis in the rat by inhibitors of glycogen synthase kinase-3β, Br. J. Pharmacol., 147 (2006) 575–582.
[46] E. Beurel, S.M. Michalek, R.S. Jope, Innate and adaptive immune responses regulated by glycogen synthase kinase-3 (GSK3), Trends Immunol. 31 (2010) 24–31.
[47] R. Barillas, I. Friehs, H. Cao-Danh, J.F. Martinez, et al., Inhibition of glycogen synthase kinase-3beta improves tolerance to ischemia in hypertrophied hearts, Ann. Thorac. Surg., 84 (2007) 126–133.
[48] A.T. Varela, A.M. Simões, J.S. Teodoro, F.V. Duarte, A.P. Gomes, et al., Indirubin-3′-oxime prevents hepatic I/R damage by inhibiting GSK-3b and mitochondrial permeability transition, Mitochondrion 10 (2010) 456–463.
[49] W. Zhao, M. Townsend, Insulin resistance and amyloidogenesis as common molecular foundation for type 2 diabetes and Alzheimer's disease, Biochim. Biophys. Acta 1792 (5) (2009) 482–496.
[50] S. Leclerc, M. Garnier, R. Hoessel, D. Marko, J.A. Bibb, et al., Indirubins inhibit

glycogen synthase kinase-3 beta and CDK5/p25, two protein kinases involved in abnormal tau phosphorylation in Alzheimer's disease. A property common to most cyclin-dependent kinase inhibitors? J. Biol. Chem., 276 (2001) 251–260.
[51] S. Zhang, X. Wang, Y. Zhang, Q. Di, J. Shi, et al., Indirubin-3′-monoxime suppresses amyloid-beta-induced apoptosis by inhibiting tau hyperphosphorylation, Neural Regen. Res., 11 (6) (2016) 988–993.
[52] C.J. Yuskaitis, R.S. Jope, Glycogen synthase kinase-3 regulates microglial migration, inflammation, and inflammation-induced neurotoxicity, Cell. Signal. 21 (2009) 264–273.
[53] M. Zhang, Y. Wu, L. Xie, C. Teng, F. Wu, K. Xu, et al., Isoliquiritingenin protects against blood-brain barrier damage and inhibits the secretion of pro-inflammatory cytokines in mice after traumatic brain injury, Int. Immunopharmacol., 65 (2018) 64–75.
[54] V.R. Konda, A. Desai, G. Darland, J.S. Bland, M.L. Tripp, Rho iso-alpha acids from hops inhibit the GSK-3/NF-B pathway and reduce inflammatory markers associated with bone and cartilage degradation, J. Inflamm. 6 (26) (2009) 1–9.
[55] M. Martin, K. Rehani, R.S. Jope, S.M. Michalek, Toll-like receptor-mediated cytokine production is differentially regulated by glycogen synthase kinase 3, Nat. Immunol. 6 (2005) 777–784.
[56] P.A. Baeuerle, D. Baltimore, NF-kappa B: ten years after, Cell 87 (1996) 13–20.
[57] M.Y. Takashi, The nuclear IkB family of proteins controls gene regulation and immune homeostasis, Int. Immunopharmacol. 28 (2) (2015) 836–840.
[58] X. Zhang, G. Zhang, H. Zhang, M. Karin, H. Bai, D. Cai, Hypothalamic IKKb/NF-kB and ER stress link Overnutrition to energy imbalance and obesity, Cell 135 (2008) 61–73.
[59] S.Y. Park, M.L. Jin, Y.H. Kim, Y. Kim, S.J. Lee, Anti-inflammatory effects of aromatic-turmerone through blocking of NF-κB, JNK, and p38 MAPK signalling pathways in amyloid β-stimulated microglia, Int. Immunopharmacol. 14 (1) (2012) 13–20.
[60] X. Song, Q. Yu, X. Dong, H.O. Yang, K. Zeng, J. Li, P. Tu, Aldose reductase inhibitors attenuate β-amyloid-induced TNF-α production in microglia via ROS-PKC- mediated NF-κB and MAPK pathways, Int. Immunopharmacol. 50 (2017) 30–37.
[61] Y. Hu, Z. Zeng, B. Wang, S. Guo, Trans-caryohyllene inhibits amyloid β (Aβ) oligomer-induced neuroinflammation in BV-2 microglial cells, Int. Immunopharmacol. 51 (2017) 91–98.
[62] M. Samuelsson, L. Fisher, K. Iverfeldt, Beta-amyloid and interleukin-1beta induce persistent NF-κB activation in rat primary glial cells, Int. J. Mol. Med. 16 (3) (2005) 449–453.
[63] J. Kim, G. Park, Indirubin-3-monoxime exhibits anti-inflammatory properties by down-regulating NF-kB and JNK signaling pathways in lipopolysaccharide-treated RAW264.7 cells, Inflamm. Res. 61 (2012) 319–325.
[64] O. Choi, Y.H. Cho, S. Choi, S.H. Lee, S.H. Seo, H.Y. Kim, et al., The small molecule indirubin-3′-oxime activates Wnt/b-catenin signaling and inhibits adipocyte differentiation and obesity, Int. J. Obes., 38 (2014) 1044–1052.
[65] L. Ho, C. Pieroni, D. Winger, D.P. Purohit, P.S. Aisen, et al., Regional distribution of cyclooxygenase-2 in the hippocampal formation in Alzheimer's disease, J. Neurosci. Res., 57 (1999) 295–303.
[66] Z.S. Kherani, R.N. Auer, Pharmacologic analysis of the mechanism of dark neuron production in cerebral cortex, Acta Neuropathol. 116 (2008) 447–452.
[67] S.H. Ahmadpour, H. Haghir, Diabetes mellitus type 1 induces dark neuron formation in the dentate gyrus; a study by Gallyas' method and transmission electron microscopy, Romanian J. Morphol. Embryol. 52 (2) (2011) 575–579.
[68] A. Zsombok, Z. Tóth, F. Gallyas, Basophilia, acidophilia and argyrophilia of “dark”(compacted) neurons during their formation, recovery or death in an otherwise undamaged environment, J. Neurosci. Methods 142 (2005) 145–152.
[69] H.J. Qiao, R.C. Koya, K. Nakagawa, H. Tanaka, H. Fujita, M. Takitmoto, N. Kuzamaki, Inhibition of Alzheimer's amyloid-peptide-induced reduction of mitochondrial membrane potential and neurotoxicity by gelsolin, Neurobiol. Aging 26 (2005) 849–855.
[70] C. Behl, Apoptosis and Alzheimer's disease, J. Neural Transm. 107 (11) (2000) 1325–1344.
[71] D.A. Linseman, B.D. Butts, T.A. Precht, R.A. Phelps, S.S. Le, et al., Glycogen synthase kinase-3beta phosphorylates Bax and promotes its mitochondrial localization during neuronal apoptosis, J. Neurosci., 24 (2004) 9993–10002.
[72] S. Snigdha, E.D. Smith, G.A. Prieto, C.W. Cotman, Caspase-3 activation as a bifurcation point between plasticity and cell death, Neurosci. Bull. 28 (1) (2012) 14–24.
[73] M. D'Amelio, M. Sheng, F. Cecconi, Caspase-3 in the central nervous system: beyond apoptosis, Trends Neurosci. 35 (11) (2012) 700–709.
[74] W. Pratchayasakul, S. Kerdphoo, P. Petsophonsakul, A. Pongchaidecha, N. Chattipakorn, et al., Effects of high-fat diet on insulin receptor function in rat hippocampus and the level of neuronal corticosterone, Life Sci., 88 (2011) 619–627.
[75] D. Luo, X. Hou, L. Hou, M. Wang, S. Xu, C. Dong, X. Liu, Effect of pioglitazone on altered expression of Aβ metabolism-associated molecules in the brain of fructose-drinking rats, a rodent model of insulin resistance, Eur. J. Pharmacol. 664 (2011) 14–19.
[76] R.A. Anderson, B. Qin, F. Canini, L. Poulet, A.M. Rouss, Cinnamon counteracts the negative effects of a high fat/high fructose diet on behavior, brain insulin signaling and Alzheimer-associated changes, PLoS One 8 (2013) 1–12 e83243.